

Multiparametric Imaging of Bone Architecture: a Cadaveric Study

¹Allen, N; ¹Weiss, K L; ¹Numan, S; ¹Hazenfield, M; ¹Ying, J; ¹Huston, R; ¹Watts, N; ¹Nilesh, B; ¹Strunk R; ¹Renner, L; ¹Lemen, L C; ²Chmielewski, P; ²Blanton, C; ²Gross, G; ²Dufresne, T; ²Nurre, J; and ²Borah, B.

¹University of Cincinnati, Cincinnati, OH, ²Procter & Gamble Pharmaceuticals, Health Care Research Center, Mason, OH

Introduction: Since osteoporosis is a systemic disease, it might be assumed to have similar degenerative effects on microarchitecture across osseous sites. Architectural measurements from the appendicular skeleton, such as the distal radius, which are more easily obtained in vivo, could then be used as surrogate markers of axial skeletal architecture. The hypotheses tested include: 1) the presence of vertebral fractures will correlate negatively with vertebral strength and 2) the microarchitecture of the distal radius and vertebral bodies will correlate with vertebral strength.

Methods: Subjects: Five cadavers donated for medical science research were studied, after formalin fixation. Thoracic and lumbar vertebrae were dissected in each cadaver and used in image analysis and strength testing. QCT, μ CT, and destructive testing were completed for each specimen. Mixed effect models were used to compare strength measures and SDI. Mixed linear models with a random effect were used to assess relationships between strength measures and architectural measures, using a random effect to account for within subject correlation of repeated observations.

Results: Three of 5 subjects had minor/moderate fractures (with SDI = 1.5, 2 and 3 respectively) and 2 others had severe fracture (both with SDI=14). Mean \pm SE of vertebral strength was 220.9 ± 19.3 (lb/in²) for minor/moderate fracture cases and 92.1 ± 22.0 lb/in² for severe fracture cases respectively (p=0.001). Strength was positively correlated with BV/TV and Conn Dens with slope \pm SE's being 17.7 ± 7.1 (p=0.033) and 89.6 ± 29.2 (1/mm³) (p=0.012); and negatively correlated with SMI and Star volume with slope \pm SE's being -90.4 ± 31.7 (p=0.017) and -0.99 ± 0.3 mm³(p=0.003) respectively. When strength and BMD were compared, the relationship was not significant with slope \pm SE being 0.38 ± 0.32 and a p=0.261. Finally, weak correlation was demonstrated when comparing the strength measures from the vertebrae to architectural measures from the radius (p's >.05).

Discussion: As hypothesized, there was a very high correlation between prevalent vertebral fractures and decreased vertebral strength. Vertebral architecture was a much better predictor of vertebral strength than distal radius microarchitecture, which was only weakly correlated. An increase in sample size is needed to further validate these results as a small sample size is a limitation of this study.

Characterization of Signaling Properties of the HCMV-Encoded G Protein Coupled Receptor US28 and Analysis of its Contribution to Viral Induced Atherosclerosis

Joanna M. Brenneman, Melissa P. M. Stropes, William E. Miller

Department of Molecular Genetics, University of Cincinnati College of Medicine, Cincinnati, OH 45267

The herpesvirus, human cytomegalovirus (HCMV), has been shown to induce vascular smooth muscle migration, and therefore, is a likely contributor to the development of vascular diseases such as atherosclerosis. Atherosclerosis involves a sequence of inflammatory events that ultimately result in a narrowing of the walls of arterial vessels by the formation of fibrous plaques. The release of chemoattractant molecules (such as RANTES) by LDL engorged macrophages and the subsequent migration of smooth muscle cells from surrounding areas into the vessel intima is associated with the formation of an advanced atherosclerotic lesion. It has been demonstrated that this process is augmented by infection of surrounding smooth muscle cells with HCMV, and therefore, the expression of viral gene products is implicated in the formation of vascular disease. HCMV encodes a G protein-coupled receptor (GPCR), US28, which binds to the chemokine RANTES and demonstrates various modalities of cell signaling, including activation of phospholipase C- α (PLC- α), release of calcium from intracellular stores, and activation of numerous transcription factors. The US28 gene product is the suspected culprit of HCMV-associated atherosclerosis, as US28 activity has been demonstrated to result in arterial smooth muscle cell migration. In this study we have investigated the signaling properties of various US28 mutants in smooth muscle cells infected with HCMV. Unexpectedly, the N-terminal chemokine binding domain is not required for PLC- α signaling and RANTES has no effect. Conversely, this chemokine binding domain and stimulation with RANTES is required for calcium release from intracellular stores. We have also investigated the effects of US28 on signaling via endogenous lysophosphatidic acid (LPA) receptors. LPA is a component of oxidized LDL and like other chemoattractant molecules has been demonstrated to play a role in the development of atherosclerotic plaques. Interestingly, the data indicate that US28 can enhance signaling via endogenous LPA receptors. Taken together, our results indicate that US28 induces a variety of signaling events in smooth muscle cells; some dependent on agonist and some independent of agonist. We are currently investigating how these US28 signaling events contribute to the pathogenesis of HCMV induced atherosclerosis.

Identification of a Previously Unrecognized Biomarker of Contrast Induced Nephropathy

David Dow, Michael Bennett, Prasad Devarajan

Division of Nephrology and Hypertension, Cincinnati Children's Hospital Medical Center

Introduction: Contrast induced nephropathy (CIN) is the third leading cause of hospital acquired Acute Kidney Injury (AKI), accounting for 10-15% of AKI in hospitalized patients. Earlier, more sensitive biomarkers that could be detected through a simple urine test would make it more feasible to screen all patients undergoing procedures involving contrast administration to determine their risk for CIN. This would allow for the commencement of prophylactic treatments and closer monitoring in the days following contrast administration.

Hypothesis and Aims: We conducted a cross-sectional study in children undergoing elective cardiac catheterization. We identified a 4631 Da protein that appears in the distinct pre-procedural urinary proteomic profile in subjects who subsequently develop CIN. Based on the literature and our previous results, we hypothesized that this protein is an amino acid variant of human beta-defensin-1, an antimicrobial peptide that is a component of the innate immune response.

Methods: In this study, we used surface-enhanced laser desorption/ionization time-of-flight mass spectrometry (SELDI-TOF-MS) to analyze urine from children undergoing contrast administration. Upon identifying the presence of the 4631 Da peak, the urine was exposed to anti-HBD-1 coated beads and again subjected to SELDI to determine if this marker was a variant of human beta defensin-1.

Results: In pre-procedural urine, the 4631 Da protein was bound by the antibody with significant intensity relative to known amino acid variants of HBD-1.

Conclusion: Continuation of ongoing urinary biomarker studies will be needed to validate HBD-1 variants as markers of CIN and to discover and identify additional biomarkers for this potentially devastating condition.

Molecular Mechanisms of Autoimmune Disease

Mohammed Fadlalla, Yaron Tomer

Division of Endocrinology, University of Cincinnati

Seminal work by Yaron Tomer, M.D., has revealed various single nucleotide polymorphisms (SNP) that influence the likelihood of acquiring Autoimmune Thyroid Disease (AITD). Through whole genome screens and associated studies, these SNPs were found to reside in the *thyroglobulin (Tg)*, *MHC II*, *CD 40*, and *CTLA-4* genes. Furthermore, deeper analysis has unearthed striking genetic interactions between disease causing SNPs in the *Tg* and *MHC II* gene, which may mirror a *bona fide* biochemical interaction between the protein products of these genes. My work in the summer focused heavily on developing assays to better elucidate these molecular mechanisms and demonstrate their correlation to AITD.

The first part of my project focused entirely on a SNP in the promoter element of the *Tg* gene. A promoter luciferase system was created and utilized as a way of testing an individual SNP's contribution to the activity of the *Tg* promoter. Interestingly, a disease-causing variant at position -1690 displayed an enhanced activity relative to its protective counterpart. Moreover, the disease causing SNP was shown to harbor an Ets-responsive element. Additional transcription factors that may bind to this region in both the disease causing SNP as well as the protective allele are feverishly being explored using a Yeast-One-Hybrid system. Results from this screen could potentially yield definitive molecular culprits for this SNP's propensity for causing AITD.

In the second part of my study, a reverse immunological approach was employed to identify disease-causing variants of the *Tg* protein. From a list of putative peptides generated *in vivo* by endoprotease digestion, two were selected for further experimentation; one spanning a known disease causing SNP, while the other encompassed a potential iodination site. Both variants of the peptide were synthesized, representing changes in amino acid sequence and iodination state. Using a bacterial recombinant system, which I showed to bind at least as effectively as cell-cultured molecule, empty *MHC II* molecules were constructed and tested by ELISA to check their ability to bind the different peptides. Various other peptides were also assayed using this system to check their capacity as *MHC II* binders as well. Based on our assays, we report that these polymorphic distinctions can have dramatic consequences in terms of peptide binding and capture. Combined, our results shed new light on the subtleties in the relationship between DNA composition, amino acid variations, and post-translational modifications and the pathoetiology of autoimmune disease.

Effects of Valproic Acid Exposure on Synchronized Calcium Oscillations in Cortical Neuronal Cultures

Arpit Gandhi, Eric Gruenstein

Division of Molecular Genetics, University of Cincinnati

Valproic acid is a short, branched chain fatty acid commonly used in the treatment of epilepsy, bipolar affective disorder and migraine headaches. It is contraindicated in pregnancy because during the time of neural development it increases the risk of congenital abnormalities including autism. Similar effects following prenatal VPA exposure occur in rats, so they are being increasingly used as a model to study the effects of VPA on the nervous system. Currently, the mechanisms underlying VPA's beneficial and toxic effects are not well understood. In order to elucidate the mechanism of action of VPA, we decided to study its effects on neuronal networks since the formation of such networks is an important aspect of early brain development. We used an in vitro system in which fetal cortical neurons are dissociated and cultured at high density. Under these conditions they self organize into networks, which spontaneously exhibit synchronized calcium oscillations. The frequency and amplitude of the oscillations are a measure of the extent and effectiveness of network function.

We found that acute addition of VPA to these spontaneously oscillating networks substantially reduced the frequency of the oscillations at normal therapeutic doses while at somewhat higher doses the amplitude was also reduced. When Mg^{2+} , a physiological regulator of NMDA receptors was removed from the medium, the order of VPA effects was reversed, so that the amplitude of calcium oscillations was reduced at therapeutic doses while effects on their frequency required higher doses.

We also found that exposure of neurons to therapeutic levels of VPA for just 24 hours during their second day in culture gave rise to a significant *increase* in the frequency of calcium oscillations in cultures as old as several weeks. Furthermore, somewhat higher levels of VPA during this early 24-hour period significantly decreased the cell count in neuronal cultures by day 7. On the other hand, chronic exposure to VPA produced an increased cell count, decreased oscillation frequency and increased oscillation amplitude. The range of responses to different VPA treatment protocols suggested to us that VPA is acting by a variety of mechanisms.

In order to gain some insight into the mechanism of action of acute VPA treatment, we designed protocols to study three specific ion channels: voltage gated sodium channels (VGNCs), voltage gated calcium channels (VGCCs) and NMDA receptors (NMDARs). Preliminary results of those experiments suggest that the inhibition of oscillation frequency and amplitude by acute VPA treatment is due to the blockade of VGNCs and VGCCs, but not of NMDARs.

This study validates the use of this in vitro neuronal network model for investigating the effects of VPA on neurons. It also suggests that VPA may exert its effects, at least in part, by altering network signaling processes. Further studies will be necessary to understand the exact mechanisms by which VPA is able to modulate neuronal calcium oscillations.

GM-CSF and Intestinal Epithelial Cell Survival in Ileal Crohn's Disease

Jonathan Gully, Xiaonan Han, Lee Denson, Shila Gilbert

Division of Gastroenterology & Nutrition, Cincinnati Children's Hospital Medical Center

Crohn's Disease (CD) is believed to be caused by a complex interaction between genetic susceptibility and environmental triggers leading to chronic relapsing intestinal inflammation and epithelial apoptosis. Eighty percent of CD patients have involvement of the terminal ileum. Granulocyte-macrophage colony stimulating factor (GM-CSF) promotes epithelial barrier integrity, stimulates myeloid cell anti-microbial function, and reduces disease activity in CD and experimental colitis. Recent studies have shown that ileal CD patients exhibit high levels of neutralizing GM-CSF antibodies within the range which inhibits innate immune functioning.

Independently, a subset of CD patients exhibit a hyper-responsive increase in permeability in response to non-steroidal anti-inflammatory drugs (NSAIDs), due in part to selective inhibition of the COX enzymes. NSAID exposure is recognized clinically as a common trigger for flares of disease in individuals with CD.

This study specifically tests the link between environmental, genetic, and immune factors by testing whether GM-CSF promotes ileal barrier function in mice by increasing enterocyte survival in response to gut injury with NSAIDs. It was concluded that in the absence of GM-CSF function, IEC show increased histologic injury in addition to elevated markers for apoptosis, indicating an increase in cell death. It was also determined that the GM-CSF receptor beta chain is more highly expressed in the ileum than the colon, indicating that GM-CSF could play a role in the higher prevalence of ileal CD. Therapeutic agents for patients with CD are limited by a lack of animal models directly linking genetic, immune, and environmental factors. By linking these factors, this study can contribute to an overall research program that may afford an animal model appropriate for testing novel therapeutics specific to ileal CD, the largest subset of inflammatory bowel disease with the highest rate of hospitalizations, surgeries, and other morbidities.

Molecular Mechanisms of Subglottic Stenosis

PA Hartman¹, FY Thompson², and RG Elluru MD, PhD²

¹University of Cincinnati College of Medicine, ²Cincinnati Children's Hospital Medical Center department of Otolaryngology

Although well characterized in skin, little is known about the molecular pathways to wound healing in mucosal tissues. Of particular interest is the pathological wound healing that results in the formation of subglottic stenosis (SGS) causing respiratory insufficiency. SGS, a potentially fatal occurrence in which the area of the larynx and trachea beneath the vocal chords narrows following injury, is most commonly caused by prolonged intubation in the pediatric population. Through deciphering the molecular basis of SGS, new preventative measures may be discovered.

Large animal *in situ* models, while convenient for direct observation, have been plagued with high cost, mortality rates and animal discomfort. Researchers at Cincinnati Children's Hospital developed a heterotopic murine model of SGS, circumventing these issues through ectopic, syngenic transplantation of wounded laryngo-tracheal complexes (LTCs) into surgically created subcutaneous pockets in mice. This cost-effective, easily manipulated model spares the recipient mouse the morbidities associated with SGS.

This study used pharmacological agents to dissect the molecular mechanisms of SGS using the heterotopic murine SGS model. The central hypothesis was that inhibition of key players in the processes of neo-vascularization and collagen deposition will alter the process of SGS formation. Neo-vascularization and collagen deposition are known steps in wound repair and scar formation in the skin. An antibody to VEGF (a cytokine that promotes neo-vascularization) and an analogue known to inhibit collagen deposition (cis-4-hydroxy-L-proline) were each administered subcutaneously at two different doses to block suspected steps in SGS formation in separate animals. Thirty-four mice received LTC transplants. Five of these LTCs were left uninjured, and their recipients received injections of saline alone. The other twenty-nine LTCs were injured by electrocautery, and their recipients received either treatment as described above, saline or bevacizumab (a humanized anti-VEGF). We found compelling evidence that VEGF may play a protective role against SGS formation. While the evidence is not statistically significant with the current group sizes, it is suggestive enough to merit further study.

Frontal Lobe and Subcortical / Cortical Inhibitory Deficits and Neuropsychological Performance in ADHD Children

Matthew D. Johnson, Kelly Isaacs, Donald L. Gilbert, Division of Pediatric Neurology, Cincinnati Children's Hospital Medical Center.

Background: Current procedures for diagnosing Attention-Deficit/Hyperactivity Disorder (ADHD) in children involve using subjective clinical criteria. An ongoing debate is whether the use of specific neuropsychological tasks or measures can reliably indicate ADHD severity. Our objective was to evaluate two executive function tasks and compare them to parent rated symptom severity and a quantitative measure of brain inhibition.

Methods: ADHD children ages 8 to 12 were recruited by advertisement and excluded if other significant psychiatric illnesses were present. All subjects were off medication for greater than 24 hours. Symptom severity was assessed independently using the DuPaul ADHD Rating Scale: Home Version. We administered computerized versions of the Stroop task and the Mental Chronometry task (Life Science Assoc., Bayport NY). Transcranial Magnetic Stimulation was performed using two Magstim 200® stimulators (Magstim Co., New York, NY, USA) connected through a Bistim® module to a double 70 mm figure of 8 coil to measure motor cortex inhibition. Correlational analyses were performed using SPSS (Student version 16).

Results: 12 ADHD children were enrolled (mean age 9.75, 3 females, 6 qualified for TMS), mean ADHD rating (38.1 range: 11 to 52). Two versions of the Stroop were compared, and both showed lower accuracy and longer reaction times in the incongruent color-word condition. Longer Stroop reaction times correlated with greater ADHD severity (Color $r = 0.78$ $p = 0.041$; Congruent $r = 0.81$ $p = 0.027$; Incongruent $r = 0.90$ $p = 0.006$); and longer Mental Chronometry Simple and Choice Reaction Times correlated with ADHD severity (Simple $r = 0.85$ $p = 0.007$; Choice $r = 0.83$ $p = 0.011$). TMS-evoked cortical inhibition and facilitation correlated with Stroop Color Word and Interference Scores. (all $r = 0.77$ to 0.94 ; $p = 0.005$ to 0.08).

Conclusions: In ADHD children, parent-rated symptom severity correlates with poor performance on Stroop and Mental Chronometry tasks. TMS measures in motor cortex suggest a biological basis for poorer Stroop performance. These measures merit further investigation as biomarkers and clinical tools for evaluating ADHD. Acknowledgment: This research was supported by MSSRP: T35 DK 60444.

Non-invasive Detection of Cardiac Abnormalities in Duchenne Muscular Dystrophy

Narayan Kisson, Kan N Hor, MD, Janaka Wansapura, PhD, Wojciech Mazur, MD, FACC, Linda H Cripe, MD, Robert Fleck, MD, D. Woodrow Benson, MD, PhD, William M Gottliebson, MD, FACC

University of Minnesota Medical School, Minneapolis, Minnesota; Division of Cardiology, Cincinnati Children's Hospital Medical Center, Cincinnati, Ohio; Division of Radiology, Cincinnati Children's Hospital Medical Center, Cincinnati, Ohio; Division of Cardiology, The Ohio Heart and Vascular Center, Christ Hospital, Cincinnati, Ohio

BACKGROUND: Duchenne Muscular Dystrophy (DMD) is caused by deficiency in dystrophin protein and results in progressive skeletal muscle weakness and cardiac dysfunction. With advances in treatment of DMD, cardiac disease has become a significant cause of morbidity and mortality. Cardiac magnetic resonance imaging (CMR) has proved useful in characterizing the course of cardiac changes in DMD. For example, subtle changes, such as reductions in peak left ventricular myocardial circumferential strain (ϵ_{cc}), can be detected in DMD patients <10 years of age with normal ejection fraction. We hypothesized that in DMD patients the relatively increased contractility of the lateral left ventricular (LV) free wall (demonstrated previously in normal subjects) might make the region more susceptible to myocardial injury with subsequent fibrosis.

METHODS: We analyzed regional ϵ_{cc} from myocardial tagged CMR images using HARPTM software in 70 DMD males and 13 age-matched control males. The mid-papillary level LV slice was divided into 6 regions (anterior free wall, lateral free wall, etc) as per prior convention for coronary distribution pattern. ϵ_{cc} from each region was tabulated per patient. In DMD patients, myocardial delayed enhancement (MDE, a marker of myocardial fibrosis) was determined by gadolinium uptake. These results were then tabulated along with the patient's ejection fraction as well as the patient/subject's age. Patient data was subdivided based on ejection fraction and MDE status.

RESULTS: The lateral free wall regions had greater reductions in ϵ_{cc} ($\Delta\epsilon_{cc}$) when compared to controls. Furthermore, MDE was consistently detected in the regions with the greatest reductions in ϵ_{cc} in DMD patients.

CONCLUSIONS: Changes in ϵ_{cc} follow a pattern showing that the regions with greatest contractility in control subjects (the lateral free wall) are the most susceptible to injury in DMD patients, as exemplified both by the greatest reduction in regional ϵ_{cc} and the development of MDE in those regions. Furthermore, both the ϵ_{cc} reduction and MDE ultimately result in global cardiac dysfunction, as there appears to be a threshold of regional strain reduction that when crossed manifest as global functional decline.

Overexpression of *Eyes Absent Homology 4* (Eya 4) in Malignant Peripheral Nerve Sheath Tumor Cells Alters the Retinal Determination Transcription Complex and Promotes Tumorigenesis

Zheng D. Lan,¹ Jianqiang Wu,¹ Jennifer J. Kordich,¹ Deanna M. Patmore,¹ Atira Hardiman,¹ Margaret R. Wallace,² Yonatan Mahller,¹ Rashmi S. Hegde,³ Timothy P. Cripe,¹ Shyra J. Miller¹ and Nancy Ratner¹

¹ Divisions of Experimental Hematology and Cancer Biology, and ³ Developmental Biology, Cincinnati Children's Hospital Research Foundation, University of Cincinnati College of Medicine, Cincinnati, Ohio, ² Department of Molecular Genetics and Microbiology, University of Florida, Gainesville, FL 32610, USA

NF1 is an autosomal dominant disorder affecting approximately 1 in 3500 individuals worldwide. NF1 patients are at risk for malignant peripheral nerve sheath tumor (MPNST), a life threatening sarcoma. The NF1 gene product, neurofibromin, is one of a family of GTPase activating proteins (GAPs) that accelerates the hydrolysis of active Ras-GTP to inactive Ras-GDP. MPNST cells have high Ras-GTP and elevated EGFR. EGFR and HRas inhibitors slow growth of MPNST cell lines, supporting the idea that dysregulation of these signaling pathways may contribute to tumorigenesis. In order to dissect the mechanism of transformation, microarray analysis was carried out between MPNST vs. normal human Schwann cells. EYA4, a transcription factor with phosphatase activity, was upregulated 37 fold in MPNST (Miller et al., 2008).

To test the hypothesis that EYA4 overexpression is related to tumorigenesis via Ras or EGFR signaling, we knocked down EYA4 in MPNST cells using shRNA and studied expression of EYA4 and its binding partners DACH and SIX1 upon Ras and EGFR activation or suppression. EYA4 knockdown slowed cell growth, reduced cell proliferation and caused cell death. Cell migration was reduced and tumorigenesis profoundly reduced when EYA4 knockdown stable cells were injected into athymic nude mice. An EGFR selective inhibitor and dominant negative HRas reduced EYA4 and SIX1 expression and induced DACH expression, implicating the EYA4-DACH-SIX 1 complex in NF1 tumorigenesis.

A Key Role of Melanin-Concentrating Hormone in Eosinophilic Esophagitis

Elinor Lee, Carine Blanchard, Marc E. Rothenberg

Division Allergy and Immunology, Cincinnati Children's Hospital Medical Center, University of Cincinnati College of Medicine, Cincinnati, Ohio.

Background: Eosinophilic Esophagitis (EE) is a rapidly growing world-wide disease characterized by an infiltration of eosinophils in the esophagus with severe epithelial hyperplasia. Recent gene expression profiling performed on patients with EE and on healthy individuals has identified a gene encoding for Melanin-Concentrating hormone (MCH) to be up-regulated in patients with EE. If a link between MCH and EE can be established, new therapies for EE may be possible. In this study, we aimed to determine the role of MCH in various aspects of EE.

Methods: Real-time PCR analysis and immunohistochemistry were performed on normal and EE esophageal biopsies to examine expression levels of MCH and its receptor MCHR1. To assess the effects of MCH *in vitro*, esophageal epithelial cells (TE-7) were exposed to various concentrations (0 to 10000 nM) of the hormone and assessed for cellular proliferation. To test the role of MCH *in vivo*, wild-type and MCH-deficient mice were exposed intranasally to *Aspergillus fumigatus*, which had been shown previously to induce EE in mice. Their harvested esophagi were then stained and quantified for eosinophils and epithelial proliferation. Lung tissues were also obtained from WT mice and MCH-KO mice, subjected to *Aspergillus* stimulation *in vitro*, and analyzed for IL-13 expression by ELISA.

Results: Patients with active EE had elevated expression of MCH that correlated with eosinophil levels. *In vitro* assays with esophageal epithelial cells showed thus far that MCH did not induce cell proliferation. *In vivo* analysis demonstrated that MCH-KO mice were protected from aspects of experimental EE induction including eosinophil accumulation and induced expression of IL-13.

Conclusion: MCH is elevated in the esophagus of EE patients and has a key role in disease induction in an experimental model of EE.

The Immune Response to Intracerebral Hemorrhage and Effects of Heme Products.

Matthew C. Loftspring, Jeremiah McDole, Aaron J. Johnson, Joseph F. Clark
Department of Neurology, University of Cincinnati College of Medicine.

Intracerebral hemorrhage (ICH) is a stroke subtype with high rates of mortality and morbidity, with only 32% of patients surviving one year. Both heme components and the immune system have been implicated as secondary injury mechanisms after ICH. Because heme and related compounds have immunomodulatory effects it is logical to ask whether there is an interaction between these compounds and the immune system after ICH. In this report we have developed a mouse model of ICH and have utilized flow cytometry to quantitatively profile immune cell populations that infiltrate the brain at 1 and 4 days post-ICH. We have also examined the effects the heme products bilirubin and bilirubin oxidation products (BOXes) on leukocytes *in vitro* and in response to ICH. BOXes are heme-derived vasoactive molecules and they were found in the brain after ICH. Mice displayed typical markers of brain injury after ICH, including increased brain water content, apoptosis and decreased rotarod scores, a measure of motor function. At 4 d, ICH mice presented with a 2.4-fold increase in total blood derived immune cells, a 1.9-fold increase in cells of the lymphoid lineage/macrophages, a 3.4-fold increase in neutrophils and a 1.7-fold increase in CD4 T cells ($p \leq 0.05$ for all groups), compared to saline control mice; only neutrophils were elevated at 1 d. *In vitro*, bilirubin and BOXes inhibited PMA-induced superoxide production by peripheral leukocytes. *In vivo* we found differences in reactive astrogliosis between mice receiving blood and those receiving blood plus BOXes. Finally, BOXes did not affect total blood derived cells appearing in the brain after ICH. Our data suggest that CNS infiltrating inflammatory cells have a role in the response to ICH and that heme products may modulate this immune response in a complex way.

Supported by: NIH R01NS050569 and NIH T35DK060444

Dietary Intake: Obesity Phenotype and Type 2 Diabetes (T2DM) in Youth

Valerie S. Marckel BS, Jane Khoury Ph D, Elaine M. Urbina MD, Thomas Kimball MD, Lawrence M Dolan MD. Department of Pediatrics, Cincinnati Children's Hospital and the University of Cincinnati College of Medicine

Adults who have high carbohydrate intake are at increased risk for having obesity, specifically central obesity, and T2DM. While obesity is associated with T2DM in adolescents, the role of high carbohydrate intake and central adiposity in T2DM adolescents is unclear. To address this issue, we compared carbohydrate intake using a three day diet record collected in 501 youth (female 323, male 178; non-Hispanic white 181, non-white 320; age range 10-23 years,) divided into lean controls (198; BMI <85th percentile by CDC criteria), obese controls with no known disease (175; BMI ≥95th percentile), and obese individuals with T2DM (128). T2DM was defined as the presence of diabetes (fasting plasma glucose >126 mg/dl or random plasma glucose > 200) and negative serum islet cell antibody titers (glutamic acid decarboxylase, insulinoma antibody – 2, insulin autoantibodies). Dietary data was collected from two weekdays and one weekend day. To reduce within subject variance and allow more accurate quantification of individual nutrient intake (Nutrient Data System of Research for coding analysis), the average intake was calculated. Waist circumference was measured at the umbilicus. Chi-square, analysis of Variance and Covariance and correlation were used for analysis. Obese T2DM and obese controls did not differ by overall adiposity as measured by BMI-Z or central adiposity as measured by waist circumference. Total carbohydrate intake was significantly lower in obese T2DM (202 grams/day) compared to obese (232 grams/day) and lean (253 grams/day) controls (p<0.0001). Although carbohydrate intake was inversely related to BMI-z (-0.11, p<0.009) and waist circumference (-0.15, p<0.0007) overall, this association was not found within lean, obese or obese T2DM groups. We conclude that the phenotype of adiposity, overall or central, does not differentiate between youth with and without diabetes. Contrary to adults with obesity or T2DM, high carbohydrate intake is not associated with the presence of overall or central adiposity or T2DM in youth.

Targeting Genetically and Pharmacologically Rac GTPases in p190-BCR-ABL+ Acute Lymphoblastic Leukemia

Joseph Mastin^{1,2}, Abel Sánchez-Aguilera¹, Amitava Sengupta¹, Yi Zheng¹, Jose A. Cancelas^{1,3}

¹Division Experimental Hematology, Cincinnati Children's Hospital Research Foundation

²University of Cincinnati College of Medicine

³Hoxworth Blood Center, University of Cincinnati College of Medicine, Cincinnati, OH

Significance and Background: The p190-BCR-ABL oncogene is associated with B progenitor (pro-B) acute lymphoblastic leukemia (ALL) of poor prognosis and poor response to tyrosine inhibitors (Imatinib). Rac GTPases (Rac1, Rac2 and Rac3) are molecular switches that integrate extra- and intracellular signals. Rac GTPases have been shown to be activated by BCR-ABL and a small molecule inhibitor (NSC23766), can specifically target Rac activation.

Methods: First, we analyzed the proliferation and survival of p190-BCR-ABL-expressing or control (empty vector)-transduced Ba/F3 cells in presence and absence of 100 μ g/mL NSC23766 and/or 1 μ g/mL Imatinib for 4-6 days. Second, we analyzed the effect of the same drugs on p190-BCR-ABL+ expressing B-ALL (bone marrow transduction/transplantation model) developed in a Rac-deficient murine model. Leukemic cells were cultured with NSC23766 and/or Imatinib and their content in B progenitors was analyzed by pre-B Colony Forming Unit (preB-CFU) assay and Witte-Whitlock long term cultures.

Results: NSC23766 distinctly inhibited cell expansion of p190-BCR-ABL expressing Ba/F3 cells (51% vs 28% in the control group and 38% in the Imatinib-treated group). The combination of NSC23766 and Imatinib decreased further the outgrowth of p190-BCR-ABL-transduced Ba/F3 cells (73%) due to both decreased proliferation (12.8-fold reduction in frequency of cells in S-phase) and decreased survival (50% apoptosis). Mice transplanted with p190-BCR-ABL WT cells developed leukemia in a period of 6-10 weeks (median survival \sim 50 days). Pre-B colony formation ability of primary murine p190-BCR-ABL+ ALL was completely abrogated by the combination NSC23766 and Imatinib (99.7% inhibition, Figure 1). While similar levels of inhibition were observed in delayed-onset Rac2-deficient ALL (median survival \sim 90 days), Rac1/Rac2-deficient p190-BCR-ABL ALL, as expected, showed an exquisite sensitivity to NSC23766 preB CFU formation inhibition (90.5%). Reversal of compactness of colonies from Rac1/Rac2-deficient, NSC23766-treated cells and only marginal inhibition of preB CFU expansion of Rac1/Rac2-deficient ALL in White-Whitlock assays, suggested that other stroma dependent and independent signaling pathways may be activated in the absence of Rac activation.

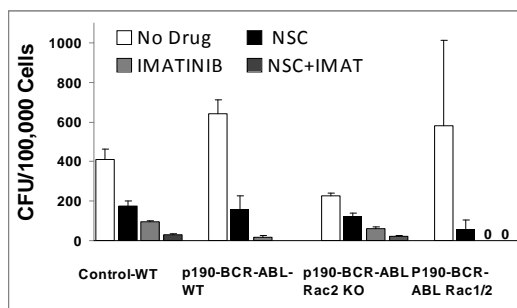


Figure 1. Genetic and pharmacological deficiency of Rac impairs p190-BCR-ABL+ leukemic progenitor outgrowth.

Conclusions: The results of this study indicate that Rac activation is necessary for the outgrowth of B-ALL induced by p190-BCR-ABL in vitro and in vivo and validate a new signaling pathway as a therapeutic target for BCR-ABL-induced B-ALL.

Role of α -MSH in Repair of UV-Induced DNA Damage, as Determined by H2AX Phosphorylation

Anne McHugh, Viki Swope, Zalfa Abdel-Malek,
Department of Dermatology, University of Cincinnati, OH

Melanoma is the deadliest form of skin cancer and is on the rise. An important paracrine factor that offers photoprotection against the carcinogenic effect of ultraviolet radiation (UV) is α -melanocortin (α -MSH). It not only stimulates eumelanin synthesis, a photoprotective pigment, but also reduces the generation of damaging reactive oxygen species, and enhances nucleotide excision repair (NER). α -MSH binds to the melanocortin 1 receptor, a G protein-coupled receptor expressed on melanocytes, causing an increase in cAMP. There are many different *MC1R* alleles that are expressed in different human populations. Some are non-functional variants that render melanocytes unresponsive to α -MSH. We explored the role of α -MSH on H2AX phosphorylation (γ H2AX) in melanocytes with different *MC1R* genotypes. H2AX is a histone protein that when phosphorylated, recruits repair enzymes to the site of damaged DNA. H2AX phosphorylation has been studied in regards to double stranded DNA breaks from ionizing radiation, but less is known about its role in repair of UVR damage. It is thought that while repairing cyclobutane pyrimidine dimers caused by UV, double stranded breaks occur, and this causes γ H2AX. Thus, we used γ H2AX as a measure of repair of UV-induced damage. To investigate the effects of α -MSH on H2AX, Western blots were run using proteins extracted from melanocytes at four time points post irradiation. Four experimental groups were used: control, α -MSH, UV, and UV+ α -MSH, and γ H2AX was detected. Flow cytometry and immunocytochemistry were also used to compare the extent of γ H2AX. The results of these experiments showed an increase in phosphorylation with UV exposure, which was augmented in the presence of α -MSH in melanocytes with functional *MC1R*. α -MSH had no significant effect on γ H2AX in cells with non-functional *MC1R*, indicating that the effect of α -MSH required functional *MC1R*. This preliminary study showing that α -MSH increases γ H2AX further confirms that α -MSH augments the repair of UV-induced DNA damage, a mechanism necessary to prevent mutations and the malignant transformation of melanocytes to melanoma

Acknowledgment:

This study was supported in part by NIH grant T35 DK 60444

Uroguanylin Gene Expression in Response to a Hypertonic Challenge in HT29-18-N2 Cells

Sekhar Padmanabhan, Mitchell Cohen, and Elizabeth Mann

Division of Gastroenterology & Nutrition, Cincinnati Children's Hospital Medical Center

Guanylate cyclase activating peptide uroguanylin (UGN) mRNA is significantly increased in HT29-18-N2 (human intestinal) cells in response to a hypertonic challenge. 5' upstream deletion analysis suggests that the UGN promoter elements that respond to hypertonicity are located between 291 and 135 base pairs upstream of the transcription start site. This sequence contains several putative hypertonicity response elements including consensus NFATC sequences. To determine the principal promoter sequence that responds to hypertonicity, oligonucleotides containing potential transcription factor binding sites were made. Nuclear extract from salt treated HT-29-18-N2 cells show increased binding to one of these oligonucleotides and competition assays using unlabeled oligonucleotides demonstrate that the nuclear extract binds preferentially to the proposed NFATC site. Mutations were introduced into the nuclear extract binding site area; however, luciferase expression of the mutated UGN promoter constructs was increased in response to hypertonic challenge. This suggests the presence of additional hypertonic response elements.

Divergent Innate and Adaptive Immunological Responses are Observed in Humans Following Blunt Trauma

Rasper AM, Kasten, KR, Goetzman HS, Adediran SG, Robinson CT, Cave CM, Lentsch AB, Johannigman JA, Solomkin JS and Caldwell, CC

The Laboratory of Trauma, Sepsis & Inflammation Research, Department of Surgery, University of Cincinnati College of Medicine, Cincinnati, Ohio 45267

The immune response to trauma has traditionally been modeled as a biphasic response. The first phase is proposed to consist of a hyper-inflammatory response, which is then followed by a second phase of hypo-inflammation. Here, we undertook a study to determine the immune response specifically to blunt trauma in male patient and healthy control cohorts. These patients and healthy controls were 18-55 years of age. After obtaining consent, peripheral blood was drawn 40-96 hours following trauma. From this blood, the phenotype and functionality of both myeloid and lymphocyte cell populations were determined. Consistent with a hyper-inflammatory response, neutrophil numbers were observed to be elevated in trauma patients as compared to healthy controls. Further, neutrophils isolated from trauma patients had increased raft formation and phospho-Akt. Consistent with this, the neutrophils had increased oxidative burst compared to healthy controls. In direct contrast, T lymphocytes isolated from trauma patients had decreased naïve T cell numbers. Upon activation with a T cell specific mitogen, trauma patient T cells were observed to have decreased T cell receptor mediated signaling. Consistent with these results, upon activation, trauma patient T cells produced less IFN-gamma as compared to those from healthy controls. Altogether, these results suggest that following trauma, there is a simultaneous and divergent immunological response to trauma. This consists of a hyper-inflammatory response by the innate arm of the immune system, while there is a hypo-inflammatory response by the adaptive arm.

Identification of Proteins Interacting with the Mitochondrial Phosphate Carrier During Necrosis Due to a Myocardial Infarction.

Elaine Reno, Jeffery Molkentin, Molecular Cardiovascular Biology, Cincinnati Children's Hospital Medical Center

During necrosis due to cardiac ischemia/reperfusion, there is excess reactive oxygen production, calcium overload, and permeabilization of the inner mitochondrial membrane, thus dissipating the electrochemical gradient and resulting in ATP depletion, increased ROS production, mitochondrial swelling, and rupture. This phenomenon of mitochondrial permeability increase is mediated by a proposed mitochondrial permeability transition (MPT) pore spanning the inner and outer mitochondrial membranes. In order to identify components interacting with a proposed element of the mitochondrial pore, a phosphate carrier, we cloned the domains of the phosphate carrier to ras. Using a yeast-two hybrid model, we began screening a cDNA library fused with a membrane localization signal. Interaction between the phosphate carrier and proposed interacting elements localizes ras to the membrane and allows yeast to grow. These clones provide additional tools to study mitochondrial permeability during necrosis, and the yeast-two hybrid model should generate components involved in the MPT pore.

Carbon Nanotubes Direct Neurite Growth: A Substrate for Neural Repair?

Erik J. Sass, Samih E. El-akkad, Keith A. Crutcher

Department of Neurosurgery, University of Cincinnati

Introduction: Failure of central nervous system (CNS) regeneration following injury occurs for many reasons, including the presence of inhibitory factors associated with myelin, glial scar formation, and lack of guidance cues for regenerating axons. In particular, there is increasing evidence that a highly aligned supporting substrate may be needed to promote accurate regeneration. Carbon nanotubes (CNT) consist of very densely packed, aligned bundles of tubular carbon molecules. The aligned structure could serve to guide growth in a particular direction. CNT can theoretically be produced with suitable geometry to allow the entry and growth of neurites (~1 μ m diameter) while excluding the entry of larger cell bodies (~10 μ m) such as astrocytes and fibroblasts that contribute to scarring at CNS injury sites.

Methods: Sympathetic chain ganglia and cortical neurons from E9-10 chick embryos were harvested and plated on CNT bundles of varying diameters and orientations to assess their ability to support neuronal attachment and neurite outgrowth. CNT arrays with various spacing between bundles were also used as templates for growth to further examine the effects of geometry and topography. Living neurons and their processes were stained with a vital dye and imaged with an inverted fluorescence microscope.

Results: Imaging revealed neuronal attachment to CNT with extensive aligned neurite outgrowth in the direction of the CNT. Neurite fascicles formed on CNT when clusters of several cell bodies were present. Neuronal attachment and outgrowth was also achieved on non-aligned CNT bundles, but the neurites did not show obvious orientation.

Discussion: The contrast between growth on aligned and unaligned CNT bundles was striking. Growth on aligned bundles appeared extensive, parallel, and with minimal branching. Incident light imaging confirmed that growth was in the direction of alignment. Growth on unaligned CNT, such as on the top of a vertical array, appeared randomly oriented. This pattern was seen in cultures of both cortical and sympathetic neurons. The results suggest that aligned carbon nanotubes might be a suitable material for supporting axonal regeneration.

(Supported by the UC Nanoscale Institute and NIH T35 DK 60444)

Subcellular Localization of Calpastatin in Cardiomyocytes Subjected to Simulated Ischemia and Reperfusion

Emily R Schoettmer, Connie J. Wagner, Steve Danzer, Jeffrey M. Pearl, Jodie Y. Duffy

Background: Cardiopulmonary bypass (CPB) is often required for the surgical repair of complex congenital heart malformations. Ischemia and reperfusion (I/R) injury to the myocardium during these repair procedures may be mediated by the proteins calpain (a calcium dependent cysteine protease) and calpastatin (the endogenous inhibitor of calpain).

Aims/Hypothesis: We aimed to localize calpastatin within cardiomyocytes undergoing simulated I/R and within cardiomyocytes treated with calpain inhibitor with or without simulated I/R. The hypothesis is that calpain and calpastatin interaction are mediated by changes in subcellular localization of calpastatin from a location around the nucleus to the cytosol.

Methods: Cardiomyocytes isolated from neonatal rats and plated on laminin-coated slides were subjected to simulated ischemia in 0.5% oxygen media without glucose for 18 hours followed by reperfusion in media with glucose at 21% oxygen for 15, 30, 60, and 120 minutes. Calpain inhibitor (2, 10, and 50 μM Z-LLY-FMK) was added 30 minutes prior to ischemia. The cells were fixed on the slide and incubated in primary antibody conjugates (Zenon Antibody Labeling, Molecular Probes) against calpain I (Alexa Fluor 594 conjugated antibody) and calpastatin (Alexa Fluor 488 conjugated antibody). Images of cardiomyocytes were captured with sequential scans on a Leica Microsystems SP5 confocal microscope using Leica Application Suite-Advanced Fluorescence confocal software (1.7.0 build 1240).

Results: In cardiomyocytes that underwent simulated I/R, calpastatin was localized around the nucleus while the cells were still ischemic (i.e. before reperfusion). After reperfusion, calpastatin was observed in localized regions in the cytosol. For untreated cells, this location change occurred by 15 minutes after reperfusion. For cells treated with 10 μM calpain inhibitor, this change occurred in some cells by 15 minutes after reperfusion and was observed in most cells by 60 minutes after reperfusion. For cells treated with 50 μM of calpain inhibitor, calpastatin was observed in the perinuclear position until 120 minutes after reperfusion. Control cells maintained in normoxic conditions did not demonstrate this change in calpastatin localization. When calpain I and calpastatin channels were overlaid, it was observed that calpain and calpastatin were colocalized after calpastatin moved to the cytosol.

Conclusions: During reperfusion, calpastatin moved to localized regions in the cytosol (possibly in association with mitochondria). In cells treated with calpain inhibitor, the time for calpastatin to move to localized regions in the cytosol was extended with increasing calpain inhibitor dose. After I/R, calpastatin and calpain I were colocalized within the cardiomyocyte. No changes in calpastatin location or colocalization with calpain were observed in control cells maintained in normoxic conditions. Future studies will aim to determine if phosphorylation or dephosphorylation of calpastatin mediates the location change with I/R. Determining how calpain and calpastatin interact during I/R can lead to deciphering the pathways of cell injury in cardiomyocytes.

Type-Specific Epidemiology and Risk Factors for Human Papillomavirus Infection in Young Women.

Tasneem Shikary BA BS, David I. Bernstein MD MA, Yan Jin PhD, Gregory D. Zimet PhD, Susan L. Rosenthal PhD, Monica McNeal, Dick Ward PhD, Jessica A. Kahn, MD MPH
Division of Adolescent Medicine and Division of Infectious Diseases, Cincinnati Children's Hospital Medical Center; University of Cincinnati College of Medicine; Indiana University, University of Texas, Medical Branch at Galveston

Objective: The objectives of this study were to: 1) determine the prevalence of any HPV, high-risk HPV, and vaccine-type HPV in sexually experienced 13-26 year-old young women within the first year post-licensing of the quadrivalent HPV-6, -11, -16, -18 vaccine, and 2) determine which demographic, gynecologic, cognitive, attitudinal, and behavioral factors as associated with high-risk and vaccine type HPV in this population.

Methods: Sexually experienced women aged 13-26 (N=409) were recruited from three clinics. All participants completed a survey instrument assessing demographic, gynecologic, cognitive, attitudinal, and behavioral characteristics and submitted cervicovaginal swabs for HPV DNA testing. Outcome measures were prevalence of high-risk type HPV and prevalence vaccine type HPV. Variables independently associated with high-risk and vaccine-type HPV were determined using unadjusted and adjusted logistic regression models.

Results: The overall prevalence of HPV was 68.4%; 59.5% were positive for ≥ 1 high-risk HPV type and were detected in 59.5% and 33.1% were positive for ≥ 1 vaccine-type HPV. The most common HPV types detected were HPV-52 (detected in 19.0%), HPV-16 (17.3%), HPV-18 (11.6%), HPV-59 (10.1%), HPV-CP610 (10.1%), HPV-6 (9.4%), HPV-66 (8.4%), HPV-51 (8.2%), and HPV-58 (8.2%). Variables independently associated with high-risk HPV infection were Black race (OR 2.03, 95% CI 1.21-3.41) and lifetime number of male sexual partners > 2 (e.g. OR for 3 vs. ≤ 1 partner 3.58, 95% CI 1.61-7.96). No variables were consistently associated with vaccine-type HPV infection.

Conclusion: In this sample of low income adolescent women the overall prevalence of HPV was high, characteristic of urban populations; however, it was significantly higher than HPV prevalence in nationally representative samples. Vaccine-type HPV were commonly detected in HPV positive women, though none of the women were infected with all four vaccine-type HPV which supports recommendations to vaccinate 13-26 year-old women even if they are sexually active. None of the variables were associated with vaccine-type HPV infection, supporting national recommendations for universal HPV vaccination.

An Imaging Study of Renal Angiomyolipoma in Patients with Tuberous Sclerosis Complex

Jason W. Steinberg, UC II, John J. Bissler, M.D.

Cincinnati Children's Hospital Medical Center, Division of Nephrology and Hypertension

Introduction: Tuberous sclerosis complex (TSC) is an autosomal dominant tumor suppressor syndrome afflicting one of every 6000 people. The disease is linked to mutations in the TSC1 or TSC2 genes. Angiomyolipomas (AMLs), tumors rich in fat, blood vessels and muscle, commonly found in TSC kidneys, increase in size with age and are a leading cause of TSC adult mortality. The extraordinarily high levels of NaCl and urea in the renal medulla versus the cortex are damaging to vulnerable DNA, interfere with DNA repair and thus possibly contribute to tumor growth.

Purpose: We performed a feasibility study of TSC patients to determine whether sufficient radiographic imaging exists to map the location of AMLs within different zones of the kidneys and to investigate if a pattern of tumor location is discernable. We expected to find a disproportionate number of AMLs in the renal medulla versus the cortex based on the hypothesis that the medulla's high osmolality facilitates tumor growth.

Methods: All patients, under the age of eighteen, were selected for this study from the Tuberous Sclerosis Clinic of Cincinnati Children's Hospital Medical Center, having fulfilled the clinical diagnostic criteria for TSC with abdominal or retroperitoneal imaging electronically accessible. AMLs larger than 4 mm and exclusively located within either a well-demarcated cortex or medulla were scored and measured for size, side, dimensional position and relative distance from papilla (if medullary).

Results: A total of 200 AMLs were identified from 33 patients, measured and mapped to one of six zones: upper and lower polar, anterior and posterior interpolar and medial and lateral interpolar. Ultrasound (n=26), magnetic resonance imaging (n=2) and computed tomography (n=5) imaging modalities were analyzed to score the 70 medullary and 130 cortical AMLs. Imaging studies of 100 patients met the inclusion criteria for analysis. Sixty-seven imaging studies did not contain scorable data commonly due to poor cortico-medullary demarcation or significantly distorted renal architecture.

Conclusion: A greater number of tumors were found in the renal medulla of TSC patients than were expected by comparison to the normal anatomic reference data of cortex to medulla size ratios. This discovery was consistent with the hypothesis that high osmolarity contributes to tumor growth. Our investigation has established the groundwork for association studies with age, gender, biomarkers and possible therapeutic approaches, including the pharmacologic modification of the medullary osmolar gradient.

The Effects of Pluronic F68 on Cholesterol Absorption

John Szymusiak¹, Qing Yang², Dana Lee², James Heubi³, and Patrick Tso²

¹University of Cincinnati College of Medicine, Cincinnati, OH

²University of Cincinnati, Department of Pathology, Cincinnati, OH

³ Cincinnati Children's Hospital Medical Center, Department of Gastroenterology, Cincinnati OH

Background and Significance: The solubilization of cholesterol and fats by bile salts to form micelles is a key step in lipid metabolism. Pluronic F68 (Poloxamer 188), a hydrophilic detergent used in artificial blood in humans, has been proposed to compete with bile salts for the solubilization of cholesterol, altering the interaction of micelles with the brush border membrane and resulting in reduced uptake of cholesterol (but not fatty acids) by enterocytes. The primary aim of our study is to determine the effect of Pluronic F68 on intestinal uptake and lymphatic transport of fatty acids and cholesterol in bile duct intact animals.

Methods: Adult rats were prepared via the lymph fistula method. Following surgery, an infusion of lipids was prepared containing tritium labeled triglyceride, ¹⁴C labeled cholesterol, and phosphatidylcholine. Along with the lipids, each rat was infused with a 19mM solution of NaTC, F68, or 2:1 F68: NaTC at a rate of 3 mL/hr for a total of 6 hours, with lymph collected every hour. The small intestine, cecum, and large intestine were removed and washed with sodium taurocholate in normal saline, which was then collected. Finally, lipid from the mucosa of the intestine was extracted by the Folch method. An aliquot of each washing, along with an aliquot from each sample of lymph and of the extracted lipid, was taken for radioactive determination by scintillation spectrometry.

Results: We observed significantly lower cholesterol levels in the lymph of F68 treated animals versus the controls (NaTC) ($P < 0.001$). There was no significant difference in luminal cholesterol levels between F68 and control rats, while there was significantly lower levels of cholesterol in the mucosa of the F68 group versus control ($P < 0.001$). F68 led to significantly lower levels of triglyceride in the lymph compared to control rats ($P = 0.023$). However, there was no significant difference between triglyceride levels for 2:1 F68:NaTC and control rats, while the 2:1 F68:NaTC rats still showed a significant reduction in lymph cholesterol levels ($P = 0.002$) compared to controls.

Discussion: F68 is very effective in reducing cholesterol absorption in rats, and, when titrated with NaTC, does not significantly decrease absorption of triglycerides. Treatment of F68 lowers cholesterol levels in the lymph and mucosa, without having a significant effect on luminal cholesterol levels. This may be due to cholesterol being transported to the portal blood supply- a possibility with exciting potential for treatment of hypercholesterolemia.

Hepatic Low Density Lipoprotein Receptor-Related Protein (LRP-1) and HDL Metabolism

Lauren Wancata¹, Josh Basford², and David Hui²

¹University of Cincinnati College of Medicine, ²University of Cincinnati College of Medicine Dept. of Pathology

Cholesterol is essential to life as a major component of cell membranes and a precursor for steroidal hormone biosynthesis. However, elevated plasma cholesterol is a major risk factor for pathological conditions such as atherosclerosis. The receptor LRP-1 has been shown to have many roles in lipid metabolism and signal transduction, most of which are related to its binding to triglyceride-rich lipoproteins. Its contribution to regulation of reverse cholesterol transport and HDL metabolism has not been explored. In this study, we crossbred *Lrp1*^{fllox/fllox} mice with liver-specific *cre* transgenic mice to generate liver-specific LRP-1 knockout mice to examine the role of hepatic LRP1 in HDL metabolism. Plasma total- and HDL-cholesterol levels in male age matched wild type and hepatic LRP1 KO mice were compared. Metabolite levels and lipoprotein profiles were determined. Circulating levels of apolipoprotein E and AI and LCAT were quantified. Components of HDL metabolism including plasma LCAT activity, plasma-mediated cholesterol efflux from lipid-loaded macrophages, and plasma HDL clearance were assayed. Hepatic LRP1 KO mice had lower fasting total cholesterol as compared to wild type (WT=112mg/dL, KO=74mg/dL, $P \leq 0.01$) while plasma glucose, non-esterified fatty acids, and triglyceride levels were equivalent. The lower total plasma cholesterol levels observed in hLRP1 KO mice were the result of decreased HDL cholesterol. Circulating apolipoprotein E and LCAT levels were decreased in hLRP1 KO (30% and 15%, respectively) with no difference in plasma level of the major HDL protein apolipoprotein AI. In addition, hLRP1 KO mice displayed a decrease in LCAT activity (ratio of 360:490 WT=5.97, KO=5.08, $P \leq 0.05$). However, cholesterol efflux from lipid-loaded macrophages to plasma of WT and hLRP1 KO mice were similar. Intravenously injected HDL containing [³H]cholesterol ester was cleared from circulation more rapidly in hLRP1 KO mice compared to that observed in WT mice. Therefore, the lower total- and HDL-cholesterol levels observed in hLRP1 KO mice are most likely due to the more rapid HDL-cholesterol clearance rate. The decrease in LCAT protein and activity may also prevent the maturation of HDL particles, thus contributing to the accelerated clearance of smaller HDL. In conclusion, liver LRP1 participates in HDL cholesterol metabolism by accelerating its clearance from circulation. This study was supported in part by NIH grants T35 DK 60444 and RO1 DK74632.

MjCIC Cl⁻ Channels Increase Their Open Probability at High Temperatures

Julia Zhu and John Cuppoletti

Molecular and Cellular Physiology, University of Cincinnati, Cincinnati, OH

Membrane transport proteins carry out the selective transport of ions and non-electrolytes for many biological processes. Although most transport proteins operate only at physiological temperatures, the mjCIC gene product from *methanococcus jannaschii*, a hyperthermophile, retains its function at 95°C. The characteristics of this channel may lead to insights into engineering heat-resistant proteins for channel arrays and sensors. To determine how temperature affects the biophysical characteristics of the mjCIC Cl⁻ channel, the protein was cloned from genomic DNA and expressed in HEK 293 cells. Plasma membrane vesicles were then prepared from these cells. Planar lipid bilayer experiments were conducted by forming a lipid bilayer with 20mg/mL 3:1 POPE:POPG across a 100µm diameter aperture between two chambers of 50% glycerol/800mM TEACl solution and incorporating membrane vesicles expressing the mjCIC channel into the bilayer. Currents across the bilayer at different holding potentials were measured at 25°C, 60°C, and 80°C to assess the flow of chloride ions at different temperatures. Current recordings and corresponding amplitude histograms showed that mjCIC channels are mostly closed at 25°C. At 60°C, the channel is active and has higher open probability. At 80°C, many channels are open and the open probability is higher than at 60°C. In conclusion, higher temperatures significantly increase the open probability of mjCIC Cl⁻ channels. Further experiments are needed to assess the effects of temperature on other mjCIC channel characteristics and to relate channel function to structure. This study was supported by AFOSR FA9550-07-1-0257 and T35 DK 60444.